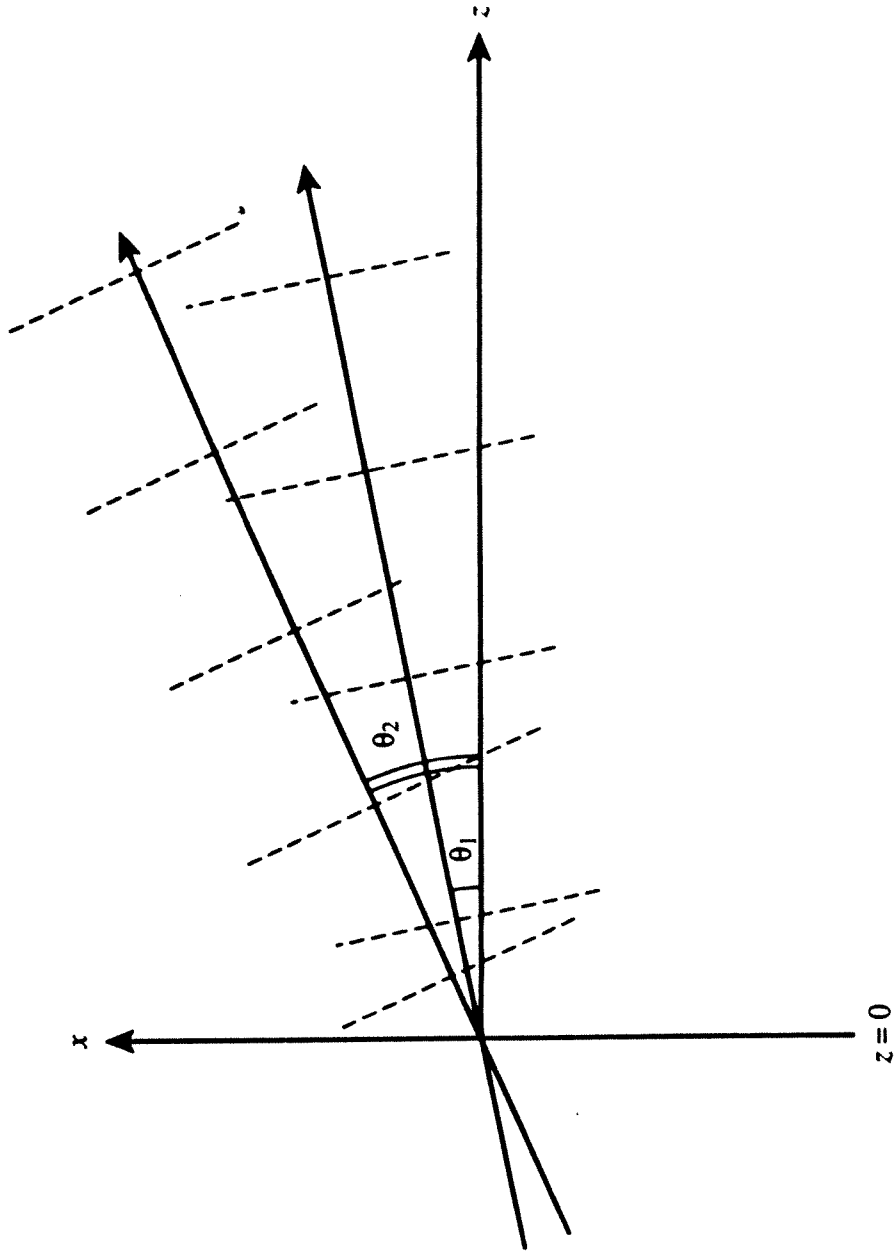


**Fig 6.1. Superposition of two plane waves travelling at different angles in the  $xz$  plane.**



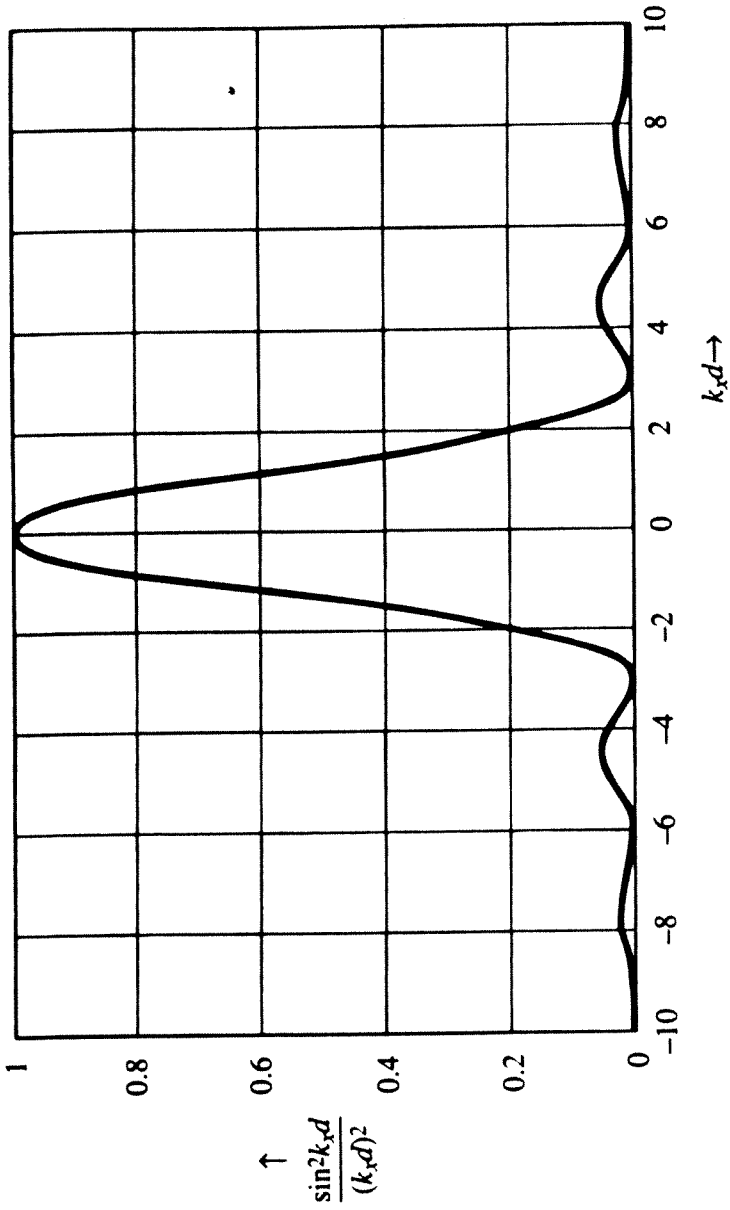


Fig. 6.2. Diffraction pattern of a single slit of width  $2d$ .

Fig. 6.3. The Airy  
diffraction pattern of  
a circular aperture.

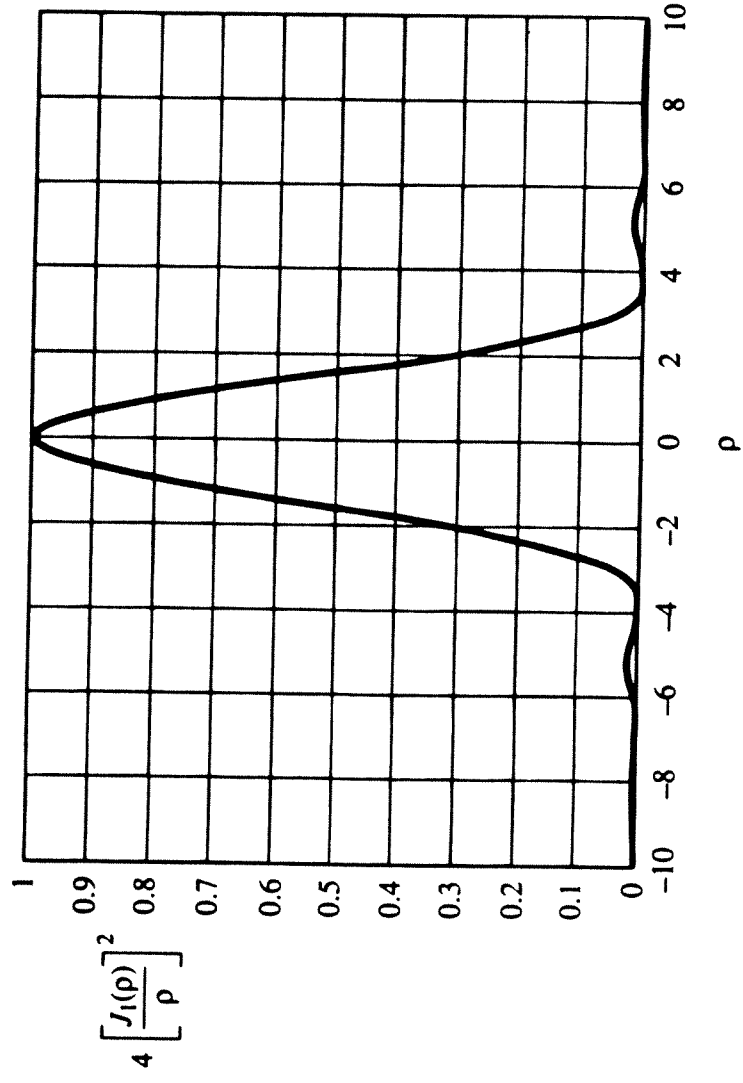
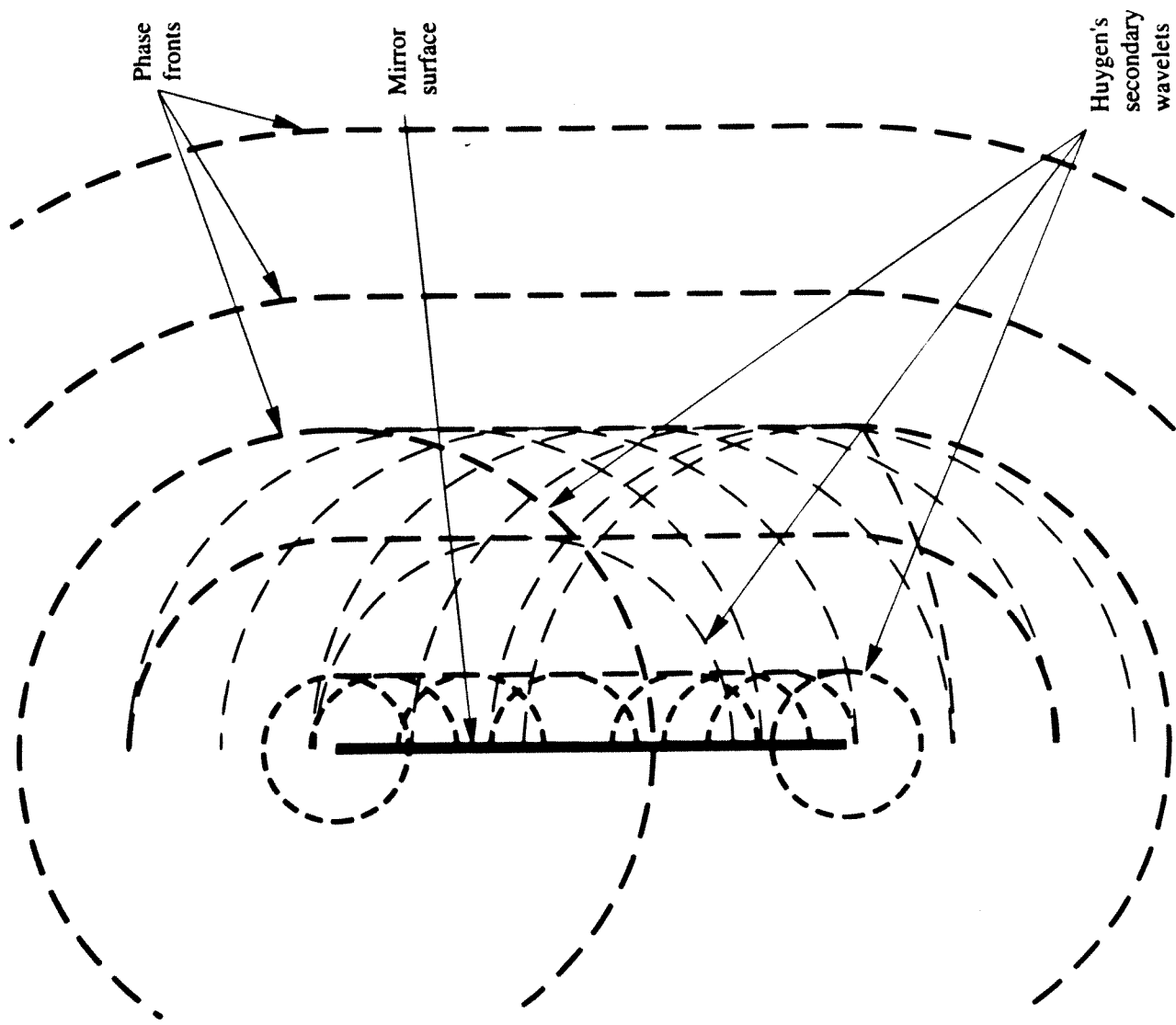


Fig. 6.4. Secondary wavelets originating from a finite plane mirror.



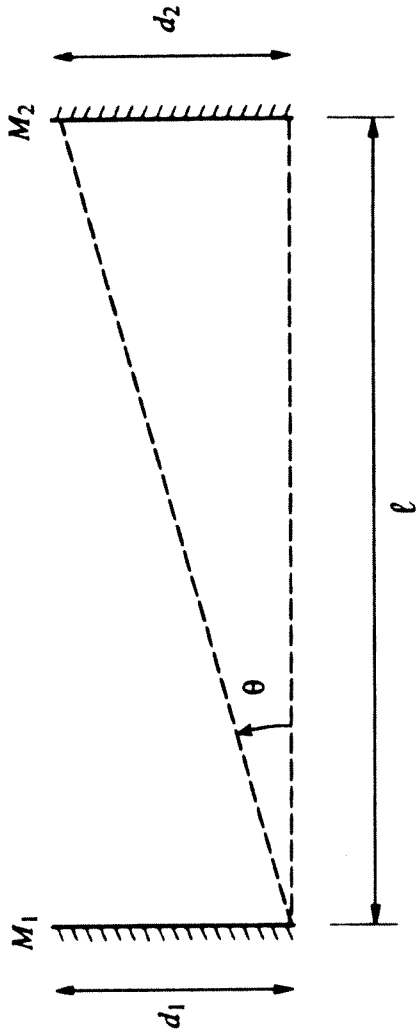


Fig. 6.5. Geometry for calculating the magnitude of diffraction effects in a laser resonator.

Fig. 6.6. Laser resonator configurations that use two spherical mirrors.  $C_1$  and  $C_2$  are the centers of curvature of mirrors  $M_1$  and  $M_2$ , respectively.

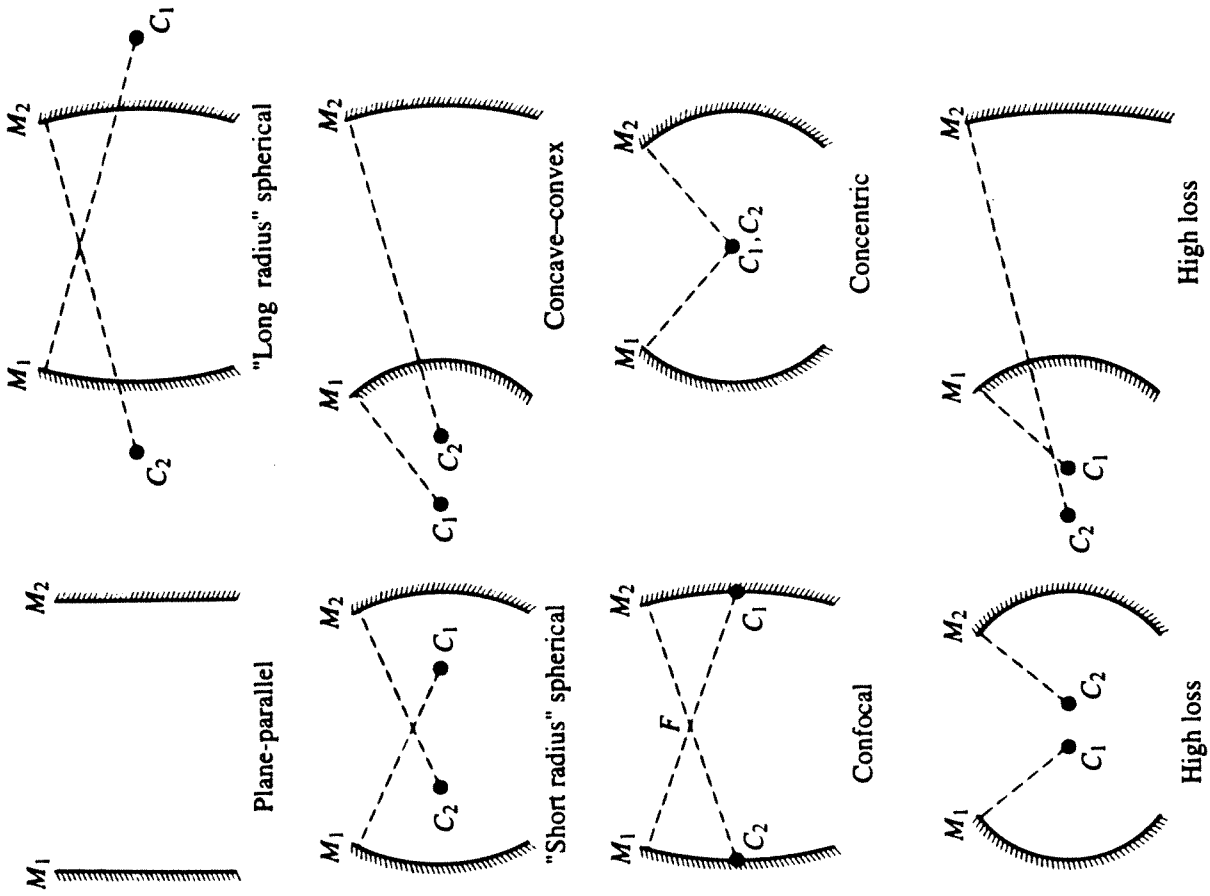


Fig. 6.7. Schematic frequencies of longitudinal modes belonging to two different transverse modes  $TEM_{mn}$  and  $TEM_{m'n'}$ .

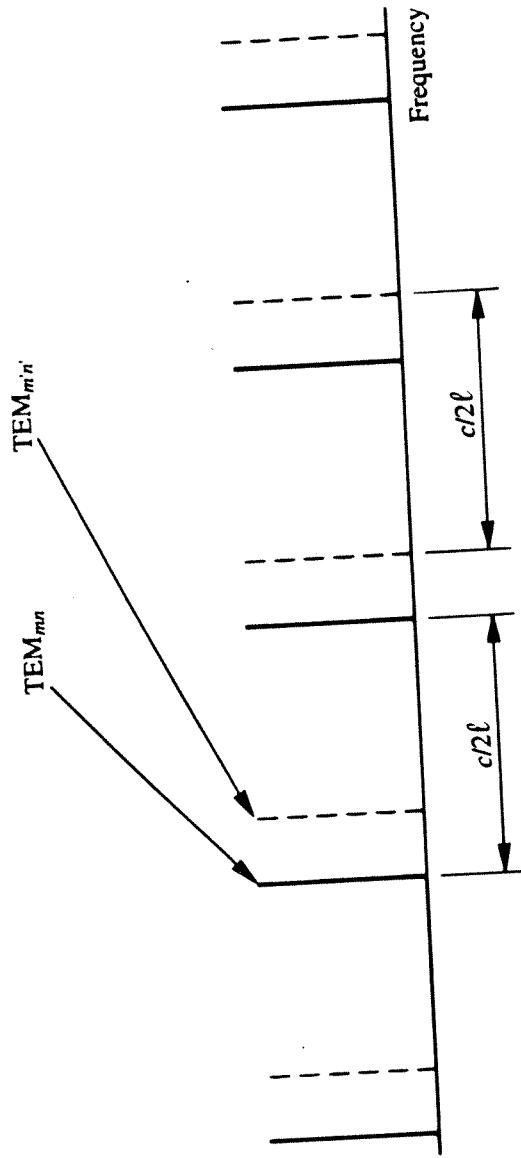


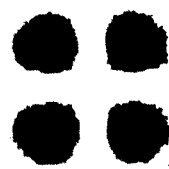
Fig. 6.8. Intensity patterns for different TEM modes possessing cartesian symmetry.



TEM<sub>20</sub>

TEM<sub>10</sub>

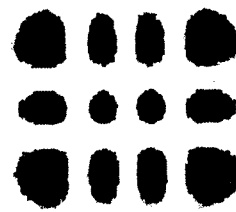
TEM<sub>00</sub>



TEM<sub>11</sub>

TEM<sub>60</sub>

TEM<sub>30</sub>

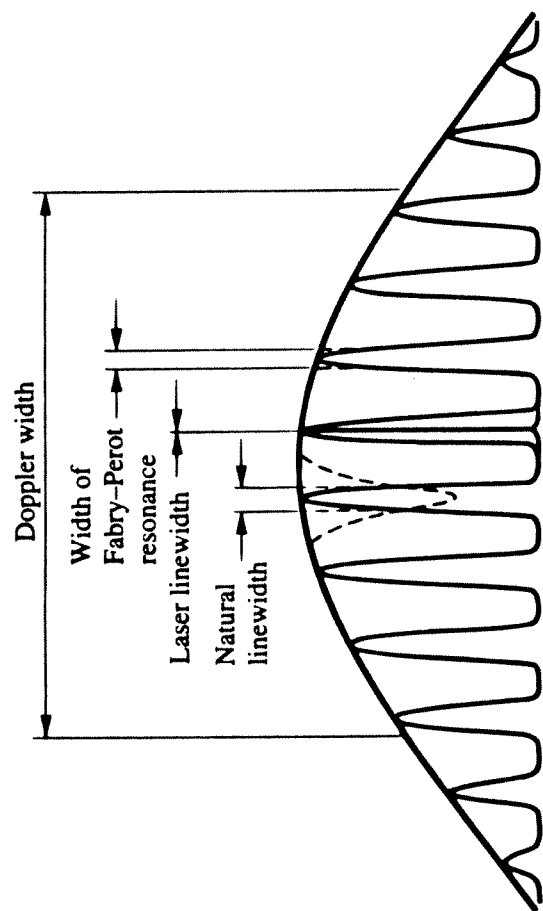


TEM<sub>23</sub>

TEM<sub>22</sub>

TEM<sub>21</sub>

Fig. 6.9. Linewidth factors in a laser.



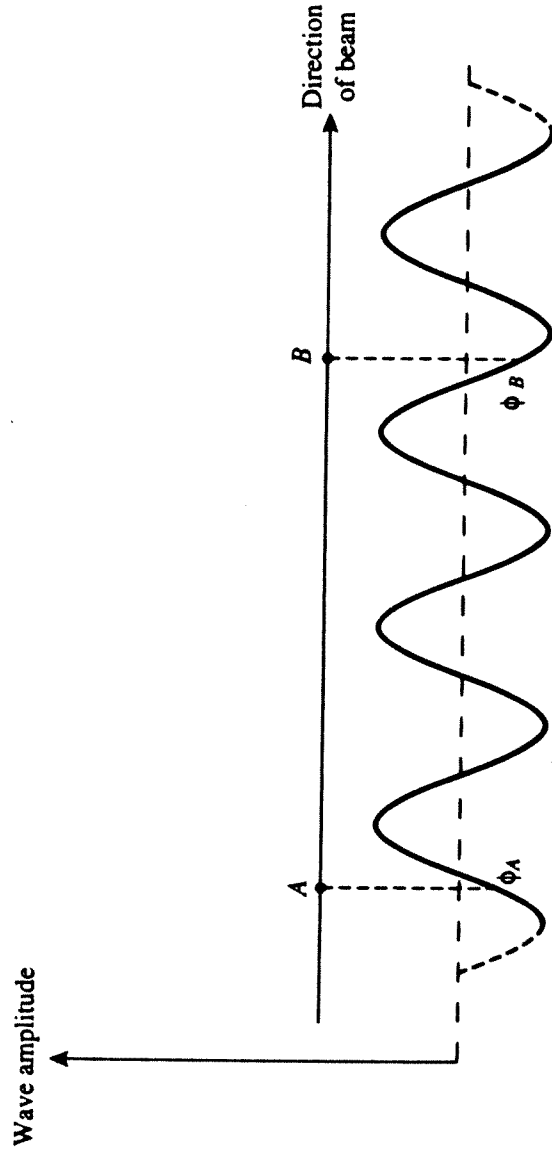


Fig. 6.10. To illustrate the concept of temporal coherence. If an unbroken wave train connects the points *A* and *B* then the phase difference ( $\phi_B - \phi_A$ ) will have a constant value.

Fig. 6.11. Michelson interferometer. Only the primary reflections are shown. Weak reflections from one surface of the beamsplitter and both faces of the compensating plate also occur unless these faces are antireflection coated. (See Chapter 14.)

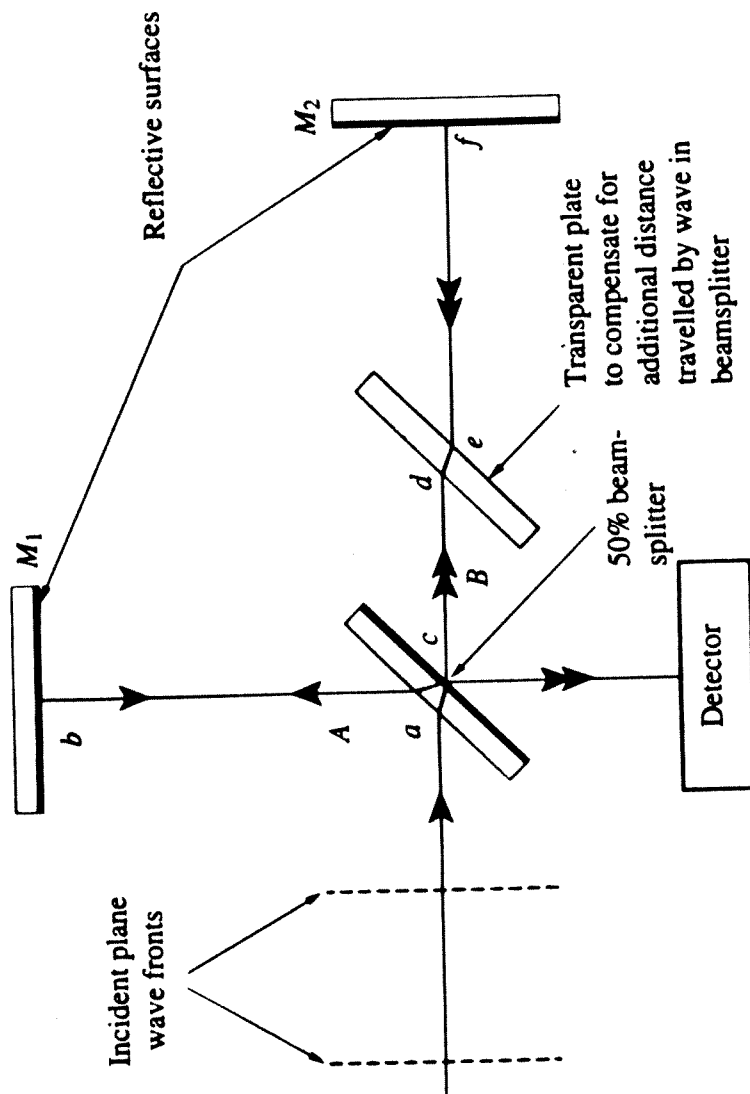


Fig. 6.12. Young's slits interference experiment to demonstrate the existence of spatial coherence in a phase front.

